Joint Timing Epoch Tracking and Channel Estimation for Alamouti Space-Time Coding in Rayleigh Fading MIMO Channels

Pawel A. Dmochowski, Peter J. McLane
Department of Electrical and Computer Engineering
Queen's University, Kingston, ON, K7L 3N6, Canada
Email: {dmochowp,mclane}@ee.queensu.ca

***Abstract*— We analyze the performance of a joint timing epoch tracking and PSAM-based channel estimation system in a frequency-flat Rayleigh fading MIMO channel. The receiver tracks a random timing drift via a timing error detector developed for $n_T = 2$ orthogonal space-time block coded M-PSK systems with an arbitrary number of receive antennas. The detector's S-curve has recently been shown to be independent of the channel state, resulting in system very robust in poor channel conditions. We evaluate the receiver's tracking capabilities in conjunction with channel estimation and study the effects of the delay inherent to PSAM interpolation systems. Symbol error rate performance for a QPSK system is presented, with the results showing negligible performance degrad**

I. Introduction

The emergence of multiple input multiple output (MIMO) systems has allowed for an increase in the data rate and the capacity of wireless links. In particular, the theory of orthogonal space time block coding (OSTBC) has received a lot of attention since its development [1]–[3], due to its ability to provide maximum diversity in fading environments while maintaining low decoding complexity. As in conventional, single-antenna synchronous communications, the receiver's ability to estimate reference parameters, including timing epoch and the channel fading, is critical to the overall performance of MIMO systems.

Rapid channel fading, which characterizes mobile communications channels, must be accurately estimated and compensated for in order to achieve high quality coherent communications. Consequently, a considerable amount of effort has been invested in developing effective channel estimation techniques. One particularly popular approach has been Pilot Symbol Assisted Modulation (PSAM), developed by Sampei *et al.* [4] and Moher *et al.* [5]. In a PSAM-based system, known training symbols are periodically inserted into the data stream and the information extracted from them at the receiver is used to derive the channel state via interpolation. Analysis of PSAM was presented by Cavers in [6], who examined the optimum (in the mean-square error sense) Wiener interpolator performance. Due to the complexity of the interpolator, and its dependence on a variety of system parameters, such as operating signal-to-ratio and the autocorrelation of the channel fading process, a number of alternative interpolation approaches have been investigated [7], [8] among others. An extension of PSAM to MIMO systems was discussed in [9].

The problem of timing acquisition in space-time coded modems was first addressed in [9], where the receiver obtained timing information by maximizing the oversampled approximated log-likelihood function (LLF), derived from orthogonal training sequences. The authors of [10] and [11] have shown that the algorithm in [9] is highly sensitive to the oversampling ratio Q, and have proposed a modification which significantly reduces the oversampling required to achieve a given MSE.

The work outlined above deals with the problem of initial timing acquisition by means of a known preamble. In this paper we focus on the task of tracking the timing in multiple antenna systems once initial acquisition has been performed. Recently, closed form expressions for the S-curve and estimation variance have derived for a timing error detector (TED) operating on OSTBC maximum likelihood (ML) detection variables [12] [13]. It was shown that the S-curve possesses a very attractive property of being independent of the channel state, and thus its performance is robust to the effects of fading.

This paper evaluates the receiver's timing tracking performance in conjunction with PSAM-based channel estimation. We examine the performance for a Wiener and a more realistic raised cosine (RC) interpolation filters. Effects of the delay inherent to PSAM systems are studied, and we show there exists an optimum value for the number of pilot interpolants depending on the rate of timing drift. Symbol error rate performance in a QPSK system is presented as well as the performance as a function of the timing drift.

The remainder of the paper is organized as follows. System overview is given in Section II. Channel estimation and timing epoch tracking for OSTBC are presented in Sections III and IV, respectively. Simulation results are presented in Section V where the error rate performance is evaluated in Section V-A and the tracking capabilities as a function of timing bandwidth are investigated in Section V-C. We conclude the paper with a summary of the findings in Section VI.

II. System Overview

We consider a communication system comprising of n_T transmit and n_R receive antennas employing orthogonal space-time block coding. The transmitter encodes N_s M-PSK information symbols and transmits them over n_T antennas in N_c time slots, resulting in a code rate of $R = N_s/N_c$.

We denote the lth $n_T \times N_c$ code block by $\mathbf{X}_l$ and its ik entry by $x_i(lN_c + k)$. Note that l is the code block index, $k = 0, \ldots, N_c - 1$ is the time slot index within the block and $i = 1, \ldots, n_T$ is the transmit antenna index. Let the mth information symbol used to encode block $\mathbf{X}_l$ be given by a_m^l, where $m = 0, \ldots, N_s - 1$. Then, $\mathbf{X}_l$ is given by the linear combination of a_m^l and their conjugates [14]

$$\mathbf{X}_l = \sum_{m=0}^{N_s-1} \Re\{a_m^l\}\mathbf{A}_m + i\Im\{a_m^l\}\mathbf{B}_m, \tag{1}$$

where the operators $\Re\{\cdot\}$ and $\Im\{\cdot\}$ return the real and imaginary parts of their arguments, and $\mathbf{A}_m$ and $\mathbf{B}_m$ are code matrices of dimension $n_T \times N_c$. For $n_T = 2$, that is the scheme proposed by Alamouti [1], $\mathbf{A}_m$ and $\mathbf{B}_m$ are given by [14]

$$\mathbf{A}_0 = \begin{bmatrix} 1 & 0 \\ 0 & 1 \end{bmatrix}, \mathbf{A}_1 = \begin{bmatrix} 0 & -1 \\ 1 & 0 \end{bmatrix} \tag{2}$$

and

$$\mathbf{B}_0 = \begin{bmatrix} 1 & 0 \\ 0 & -1 \end{bmatrix}, \mathbf{B}_1 = \begin{bmatrix} 0 & 1 \\ 1 & 0 \end{bmatrix}. \tag{3}$$

Following the encoding, data on each transmit antenna is passed through a pulse shaping filter. The pulse shaping is split between the transmitter and receiver, each employing a root raised cosine (RRC) filter denoted by $\tilde{g}(t)$. The combined raised cosine pulse is denoted by $g(t) = \tilde{g}(t) * \tilde{g}(t)$.

We assume a frequency-flat Rayleigh fading channel modeled by a matrix $\mathbf{H}$ of dimension $n_R \times n_T$. We denote each row of $\mathbf{H}$ by a vector $\mathbf{h}_j = [h_{1j}, h_{2j}, \ldots, h_{n_T j}]$. Entries h_{ij} correspond to the state of the channel from ith transmit to jth receive antenna and are assumed to be independent and identically distributed (iid) for all i and j. U-shaped power spectrum of isotropic scattering is assumed, and thus the autocorrelation of h_{ij} (for all i and j) is given by [15]

$$R_h(\xi) = \sigma_h^2 J_0(2\pi f_D \xi), \tag{4}$$

where σ_h^2 is the variance of the random process, and $J_0(x)$ denotes the Bessel function of the first kind of order zero. The quantity f_D in (4) denotes the maximum Doppler frequency.

The received signal at antenna j is given by

$$r_j(t) = \sum_{i=1}^{n_T} h_{ij}(t) \sum_{m=-\infty}^{\infty} x_i(m)\tilde{g}(t - mT) + \bar{\eta}_j(t), \tag{5}$$

where $\bar{\eta}_j(t)$ is a zero mean complex Gaussian noise with variance $\sigma_{\bar{\eta}}^2 = N_0/2$ per signal dimension. After matched filtering, $r_j(t)$ is sampled at time instants $t_n = nT + \epsilon$, where ϵ is the unknown residual timing offset after timing correction, assumed to be equal at all branches. Assuming the channel fading is sufficiently slow such that $h_{ij}(t_n) = h_{ij}(nT) \triangleq h_{ij}(n)$, the resulting samples are given by

$$y_j(n) = \sum_{i=1}^{n_T} h_{ij}(n) \sum_{m=-\infty}^{\infty} x_i(m)g(nT - mT + \epsilon) + \eta_j(n), \tag{6}$$

where $\eta_j(n)$ is used to denote the colored noise samples after match filtering. It is easily shown [9] that the noise samples are uncorrelated if sampled at the symbol rate.

Equation (6) can also be expressed as

$$y_j(n) = g(\epsilon) \sum_{i=1}^{n_T} h_{ij}(n)x_i(n) + v_j(n) + \eta_j(n), \tag{7}$$

where $v_j(n)$ is used to denote the intersymbol interference (ISI), given by

$$v_j(n) = \sum_{i=1}^{n_T} h_{ij}(n) \sum_{m \neq n} x_i(n)g(nT - mT + \epsilon). \tag{8}$$

Denoting the estimate of $\mathbf{H}$ by $\hat{\mathbf{H}}$, the ML detection variables for each information symbol m within a block, $m = 0, \ldots, N_s - 1$, are given by [14]

$$\tilde{s}_m = \frac{1}{\left\|\hat{\mathbf{H}}\right\|^2} \left[\Re\{tr(\mathbf{Y}^H\hat{\mathbf{H}}\mathbf{A}_m)\} - i\Im\{tr(\mathbf{Y}^H\hat{\mathbf{H}}\mathbf{B}_m)\}\right], \tag{9}$$

where tr denotes the trace operator, $\left\|\hat{\mathbf{H}}\right\|$ is the Frobenius norm of $\hat{\mathbf{H}}$ and $\mathbf{Y}$ is an $n_R \times N_c$ matrix with entry jn given by $y_j(n)$. The projection of $\tilde{s}_m$ onto the signal constellation then forms the detected information symbols denoted by $\hat{a}_m$.

III. Channel Estimation

The receiver estimates the channel state information using periodically transmitted orthogonal pilot sequences. For this purpose, the data is organized into frames of L_f symbols, made up of L_p pilot symbols followed by L_d data symbols. The number of OSTBC blocks in a frame is denoted by $N_b = L_d/N_c$. The resulting average data symbol energy is thus $\bar{E}_s = E_s L_f/L_d$, where E_s is the actual symbol energy.

Let $\mathbf{X}_p$ denote $n_T \times L_p$ pilot matrix, whose rows correspond to the pilot sequences transmitted by each antenna and denoted by $\mathbf{p}_i$. In order to estimate an $n_T \times n_R$ MIMO channel, the minimum length of each pilot sequence must equal to or greater than the number of transmit antennas [9]. [1]

Consider the received samples corresponding to the kth pilot sequence at receive antenna j. For notational convenience we let $\alpha_{ij}(k)$ denote the channel state for the kth pilot slot, and we assume that the channel remains constant for the duration of the pilot block, $\alpha_{ij}(k) \triangleq h_{ij}((k-1)L_f + 1) = h_{ij}((k-1)L_f + L_p)$. Using (7) it can be shown that the kth received pilot sequence is given by

$$\mathbf{y}_j(k) = g(\epsilon)\boldsymbol{\alpha}_j(k)\mathbf{X}_p + \mathbf{z}_j(k), \tag{10}$$

where $\mathbf{y}_j(k) = [y_j((k-1)L_f + 1) \ldots y_j((k-1)L_f + L_p)]$, $\boldsymbol{\alpha}_j(k) = [\alpha_{1j}(k) \ldots \alpha_{n_T j}(k)]$ and $z_j(k)$ is a vector of equivalent additive noise and ISI samples given by $z_j(k) = v_j(k) + \eta_j(k)$ for $k = (k-1)L_f + 1 \ldots (k-1)L_f + L_p$. Since

[1] Note that for OSTBC with $n_T > 2$, $N_c > n_T$, and thus the pilot and data blocks are of different durations.

the pilot sequences are orthogonal, the minimum mean square error estimate of $\boldsymbol{\alpha}_j(k)$ is given by [9]

$$\hat{\boldsymbol{\alpha}}_j(k) = \frac{\mathbf{y}_j(n)\mathbf{X}_p^H}{g(\epsilon)\|\mathbf{p}\|^2} \tag{11}$$

and the estimation error for each diversity branch is given by

$$\begin{aligned} e_{ij}(k) &= \hat{\alpha}_{ij}(k) - \alpha_{ij}(k) \\ &= \frac{\mathbf{z}_j(k)\mathbf{p_i}^H}{g(\epsilon)\|\mathbf{p}\|^2}. \end{aligned} \tag{12}$$

While the residual timing error ϵ is unknown, it is assumed that $\epsilon << 1$ and the MMSE estimate of channel state for pilot slots is obtained by approximating $g(\epsilon) \approx 1$ in (11).

The channel estimate of the data portion of the frame can be obtained via pilot interpolation provided that the normalized sampling rate of the pilots satisfies the Nyquist condition

$$\bar{f} \triangleq \frac{f_{s,p}}{2f_D} \geq 1, \tag{13}$$

where $f_{s,p} = 1/(L_f)$ is the pilot sampling rate and f_D is the maximum Doppler frequency.

The channel estimate for the nth data symbol, $-\lfloor L_d/2 \rfloor < n < \lfloor L_d/2 \rfloor$, is obtained by interpolating K nearest pilot channel estimates $\alpha_{ij}(k)$, $-\lfloor K/2 \rfloor < k < \lfloor K/2 \rfloor$, that is

$$\hat{h}_{ij}(n) = \mathbf{w}(n)^H \hat{\boldsymbol{\alpha}}_{ij}, \tag{14}$$

where $\mathbf{w}(n)$ is the column vector of K interpolation coefficients $w(n,k)$ and $\hat{\boldsymbol{\alpha}}_{ij}$ is the vector of the pilot channel estimates. It should be noted that the interpolation coefficients $\mathbf{w}(n)$ are different for each position within the frame.

The optimum coefficients, that is, those which minimize the mean square estimation error between the channel $h_{ij}(n)$ and the estimate $\hat{h}_{ij}(n)$, are given by the well known Wiener equation

$$\mathbf{w}(n) = \mathbf{R}_\alpha^{-1}\mathbf{a}(n), \tag{15}$$

where $\mathbf{R}_\alpha$ is the autocorrelation matrix

$$\mathbf{R}_\alpha = E\left\{\alpha_{ij}\alpha_{ij}^H\right\}, \tag{16}$$

and $\mathbf{a}(n)$ is the covariance vector given by

$$\mathbf{a}(n) = E\left\{h_{ij}^*\alpha_{ij}\right\}. \tag{17}$$

The (i,j)th element of $\mathbf{R}_\alpha$ can be obtained from (4), and are given by [6]

$$R_{\alpha,ij} = \sigma_h^2 J_0(2\pi f_D(i-j)L_f T) + \sigma_e^2\delta_{ij}, \tag{18}$$

where δ_{ij} denotes the Kronecker delta function. Similarly, the ith component of $\mathbf{a}(n)$ is given by [6]

$$a_i(n) = \sigma_h^2 J_0(2\pi f_D(iL_f - n)T). \tag{19}$$

It must be noted, that while the Wiener interpolator is optimal in the MMSE sense, it requires the knowledge of the channel statistics, the operating SNR as well as the Doppler frequency and is thus not suitable for practical applications. For this reason, we also consider an interpolation using a Raised Cosine filter, a use of which was examined by [7]. Among other findings, the authors in [7] determine by simulation the optimum value for the rolloff factor β_I as a function of the normalized pilot sampling rate $\bar{f}$, a result used here in the implementation of the RC PSAM interpolation.

IV. Timing Epoch Tracking

We now describe a method for timing error tracking in $n_T = 2$ OSTBC systems with an arbitrary number of receive antennas. The estimation of the timing epoch is done by means of a TED similar in form to the Mueller and Muller detector (MMD) [16], but operating on the ML detection variables given by (9). Detailed derivations of the S-curve and the estimation variance are given in [12] and [13]. In this section we summarize the properties of the TED and outline a method of timing correction using its output.

A. Timing Error Detector

1) S-curve: Consider an estimate of the timing error based on the lth OSTBC code block, i.e.,

$$\hat{\epsilon} = a_0\tilde{s}_1 - a_1\tilde{s}_0, \tag{20}$$

where a_i, $i = 0, \ldots N_s - 1$, denotes the data symbols used to encode block l, and $\tilde{s}_m$, are the ML decision metrics given by (9). For notational compactness, we have not included the block index l in the variable in (20), with the understanding that all quantities refer to the lth code block.

The S-curve is derived by evaluating the expectation of $\hat{\epsilon}$ over the information symbols a_m and noise. Using (6) and (9), one can show that the expectation $E\{\hat{\epsilon}\}$ is given by [12]

$$E\{\hat{\epsilon}\} = g_{-1}^{(\epsilon)} - g_1^{(\epsilon)}. \tag{21}$$

where $g_n^{(\epsilon)}$ denotes the samples of the overall pulse shape with an timing error ϵ,

$$g_n^{(\epsilon)} \triangleq g(nT + \epsilon).$$

From (21) we see that the detector uses the difference in threshold crossings to estimate the timing offset ϵ. The expression obtained in (21) is the same as that derived in [16] for PAM signals. It is important to note that in the presence of fading, which was not considered by [16], the detector given by (20) yields a reliable estimate regardless of the state of the channel. This is a key property making the detector very robust in poor channel conditions. The above result holds true in the sense of the statistical average over the data. In practice the timing loop approximates the statistical average with a time average over the data symbols. Note that the derivation of (21) in [12] does not take into account channel estimation errors.

2) Estimation Variance: Another key characteristic of the TED is its estimation variance, given by

$$\sigma_{\hat{\epsilon}}^2 = E\{\hat{\epsilon}\hat{\epsilon}^*\} - E\{\hat{\epsilon}\}^2. \tag{22}$$

As with the evaluation of the the S-curve, the expectation in (22) is taken over data a_m and the noise. The derivation of

the variance is rather involved, with the details presented in [13]. Defining

$$\chi_{mn} \triangleq \sum_{j=1}^{n_R} h_{mj} h_{nj}^*, \ m,n = 1,2 \tag{23}$$

the solution can be shown to be given by [13]

$$\begin{aligned}
\sigma_{\hat{\epsilon}}^2 &= \frac{2}{\|H\|^4} \left\{ \left(\chi_{11}^2 + \chi_{22}^2 + 2\left|\chi_{12}\right|^2 \right) \sum_n {g_n^{(\epsilon)}}^2 \right. \\
&+ 2\left(\chi_{11}\chi_{22} - \left|\chi_{12}\right|^2 \right) \left(\sum_n {g_{2n}^{(\epsilon)}}^2 - \sum_n g_{2n+1}^{(\epsilon)} g_{2n-1}^{(\epsilon)} \right) \\
&- \left(\chi_{11}^2 + \chi_{22}^2 \right) \left({g_0^{(\epsilon)}}^2 + g_1^{(\epsilon)} g_{-1}^{(\epsilon)} \right) \\
&- \chi_{11}\chi_{22} \left(2{g_0^{(\epsilon)}}^2 - {g_1^{(\epsilon)}}^2 - {g_{-1}^{(\epsilon)}}^2 \right) \\
&+ \left. \rho\chi_{12}^2 \left(g_1^{(\epsilon)} + g_{-1}^{(\epsilon)} \right)^2 + \left(\chi_{11} + \chi_{22} \right) \sigma_{\eta'}^2 \right\} \\
&- \left(g_{-1}^{(\epsilon)} - g_1^{(\epsilon)} \right)^2,
\end{aligned} \tag{24}$$

where $\rho \triangleq E\left\{a_m^2\right\}$. It can be shown that

$$\rho = \begin{cases} 1, & BPSK \\ 0, & MPSK, M > 2 \end{cases}. \tag{25}$$

Finally, $\sigma_{\eta'}^2$ in (24) is given by

$$\sigma_{\eta'}^2 = \begin{cases} N_0/2, & BPSK \\ N_0, & MPSK, M > 2 \end{cases}. \tag{26}$$

In the case of BPSK, the variance of the TED contains noise of one signal dimension only. This is because when evaluating the OSTBC decision metrics (9), the imaginary components are disregarded, and the noise associated with them does not propagate to the TED.

Unlike the expression for the S-curve, (24) is dependent on the channel state. It is not possible to obtain an analytical expression for the expectation over the fading, mainly due to the denominator involving the channel state. Averaging of (24) over the fading must thus be carried out via simulation, as was done in [13].

B. Timing Error Correction

Due to pilot interpolation, channel estimates are generated on a frame-by-frame basis. Specifically, after pilot for frame k' has been received, channel state information for frame $k = k' - \lceil K/2 \rceil$ are available. The receiver then decodes all N_b OSTBC blocks in frame k, and thus is able to obtain the corresponding TED estimates via (20). These TED outputs are used to correct the timing phase for frame $k+1$. Thus, as a result of pilot interpolation, the timing estimation and correction are delayed by $\lceil K/2 \rceil$ frames.

Consider data block l, transmitted as part of frame k. Let the residual timing error for that block be expressed as

$$\epsilon_l = \tau_l - \hat{\tau}_k,$$

where τ_l is the timing delay relative to the receiver time axis and $\hat{\tau}_k$ is the timing correction introduced for frame k. To minimize the effects of noise, the timing error estimates $\hat{\epsilon}_l$ for each data block in frame k are passed through a first-order IIR filter. We denote the filtered error estimate by $\hat{\epsilon}'_l$, where

$$\hat{\epsilon}'_l = \alpha\hat{\epsilon}'_{l-1} + (1-\alpha)\hat{\epsilon}_l. \tag{27}$$

The filter output for $l = kN_b$, that is the last filter output in frame k, is used to compute the timing correction for the next frame. If $\hat{\epsilon}'_l$ exceeds some threshold value ϵ_{th}, the timing correction $\hat{\tau}_l$ is adjusted by a fraction of the symbol interval T/Q, depending on the polarity of the error estimate,

$$\hat{\tau}_{k+1} = \begin{cases} \hat{\tau}_k + T/Q, & \hat{\epsilon}'_k > \epsilon_{th} \\ \hat{\tau}_k - T/Q, & \hat{\epsilon}'_k < -\epsilon_{th} \end{cases}. \tag{28}$$

V. Simulation Results

We present simulation results evaluating the performance of the TED in conjunction with PSAM channel estimation as described by Sections III and IV. We consider symbol error rate for Wiener and RC interpolation, and study the effects of the delay associated with large K. Finally, the range of timing drift bandwidth tracked by the receiver is determined.

The data was organized in frames of $L_p = 2$ pilot slots, followed by 4 data code blocks. The resulting pilot spacing of $L_f = 10$ is adequate for estimation of channel with a normalized Doppler frequency well in excess of $f_D T = 0.01$ considered here. The data symbols were encoded using the Alamouti code matrices given in (1), (2) and (3), before being passed through an RRC pulse shaping filter with a rolloff factor of $\beta = 0.35$. We consider frequency-flat Rayleigh fading, independent on each branch, with a normalized Doppler frequency $f_D T = 0.01$. The data was corrupted by additive white Gaussian noise.

At the receiver, the signal on each branch was matched filtered and sampled. We assume that the coarse timing acquisition has been performed, which is typically done using a known training sequence. The simulations were carried out using a resolution of $T/8$, that is filtering at both the transmitter and the receiver was done using waveforms sampled at that rate. The timing drift was simulated by perturbing the sampling phase τ_l. The interval between timing slips, measured in symbol intervals and denoted by N_τ, was modeled by a Gaussian random variable, with a mean of $\bar{N}_\tau$ and with a variance of $\sigma_{N_\tau}^2$. To ensure proportional distribution of timing slip intervals for all $\bar{N}_\tau$, $\sigma_{N_\tau}^2$ was set to 10% of $\bar{N}_\tau$. The drift direction was random and equiprobable, while its size was fixed to $T/8$. The resulting mean timing error bandwidth, normalized to the symbol duration T, is given by

$$\bar{B}_\tau T = \frac{T/8}{\bar{N}_\tau T} = \frac{1}{8\bar{N}_\tau}.$$

Channel estimation was performed independently on each receiver branch by interpolation of channel states from K pilots. We consider both Wiener and RC filters. The Wiener filter coefficients were optimized for each position within the frame, the operating $\bar{E}_s/N_0$ as well as the Doppler frequency.

The Raised Cosine filter rolloff was set to $\beta_I = 0.9$, which, based on the results in [7], is suitable for normalized pilot sampling rate of $\bar{f} = 1/(L_f f_D) = 10$. As described in Section IV-B, interpolating K pilot channel estimates returns channel state information delayed by $\lceil K/2 \rceil$ frames. The data was decoded according to (9).

Since the focus of the investigation is the tracking performance, the data symbols were unknown to the receiver and the timing error estimation was performed using a decision-directed (DD) TED given by

$$\hat{\epsilon}_{DD} = \hat{a}_0 \tilde{s}_1 - \hat{a}_1 \tilde{s}_0, \tag{29}$$

where $\hat{a}_0$ and $\hat{a}_1$ are the data decisions. The TED estimate was filtered according to (27) with $\alpha = 0.9$, with the output determining the timing correction as described by (28). The timing correction threshold was set to $\epsilon_{th} = 0.25$.

A. SER Performance

We now evaluate the SER performance of 1-, 2- and 4-antenna receivers. Figures 1 and 2 show QPSK SER plots for Wiener and RC pilot interpolation, respectively. The mean timing drift bandwidth was set to $\bar{B}_\tau T = 1 \times 10^{-4}$. In addition, we provide three reference curves: ideal timing and channel estimation, ideal timing with PSAM channel estimation and finally, timing drift with ideal channel knowledge. Note that in the two cases of perfect channel knowledge, no pilot interpolation was performed and thus no delay was introduced in decoding the data and obtaining the timing information. Results corresponding to PSAM receivers take into account a 0.96 dB SNR overhead due to pilot insertion.

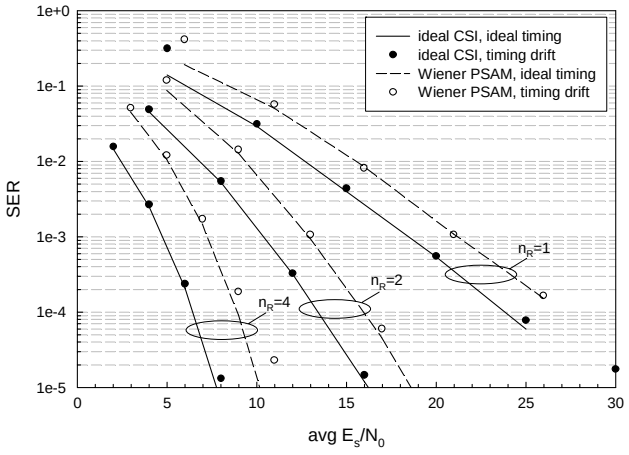

Fig. 1. QPSK SER (Wiener PSAM, $K = 9$, $L_d = 8$, $f_D T = 0.01$).

The results demonstrate that the receiver is able to track the timing variation with a very small performance drop resulting from the timing correction. By observing the reference curves, it is clear that for most part, the performance loss is due to channel estimation. The relatively low value of the error threshold ϵ_{th} results a very responsive loop, which ensures little degradation in SER. For $n_R = 2, 4$ where the operating SNR is very low, we observe the development of an error floor

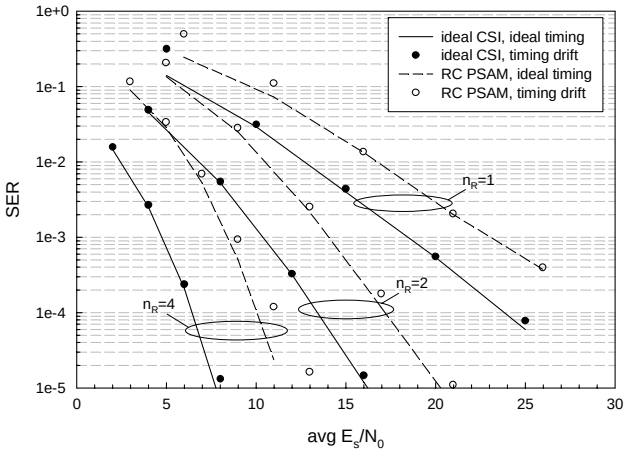

Fig. 2. QPSK SER (RC PSAM, $K = 9$, $L_d = 8$, $f_D T = 0.01$).

due to timing estimation. This is most likely caused by the fact that the errors from noisy pilot channel state information (CSI) estimates propagate to the TED estimation. One also notices poor performance at very low SNR, especially for $n_R = 1$. This is a result of noisy timing error estimates and can easily be remedied by increasing the threshold value ϵ_{th} in low SNR region. The performance for RC filtering shows similar trends, with additional performance drop of $1 - 2$ dB resulting from the non-optimum interpolation filter. We note that the only information used to compute the RC interpolation coefficients was the Doppler frequency used to select the rolloff factor.

B. Effects of Interpolation Size

As described in previous sections, interpolation introduces a delay in data decoding, which in turn results in delayed timing error information. This suggests a trade-off between poor channel estimation for small K, and long delay for large K. This trade-off is the focus of this section.

Figure 3 shows the SER as a function of K for $n_R = 2$ QPSK system at $\bar{E}_s/N_0 = 12dB$. The channel estimation was performed using a Wiener filter with L_f=10. The figure includes results for varying timing bandwidth ranging from $B_\tau T = 1 \times 10^{-4}$ to $B_\tau T = 6 \times 10^{-4}$. As a reference, a plot corresponding to a system with perfect timing is included.

The ideal timing plot shows a steady performance gain with increasing K until approximately $K = 11$. This agrees with results previously reported in [6]. As anticipated, in a system with timing tracking, the delay associated with large K results in an increase in SER. This effect is more pronounced when the timing drift is faster, as shown in plots for $B_\tau T = 4 \times 10^{-4}$ and $B_\tau T = 6 \times 10^{-4}$. While $K = 11$ or higher is optimum for smaller $B_\tau T$, for faster timing variation a value of $K = 9$ results in better performance.

C. Performance as a Function of Timing Bandwidth

Finally, we study the performance as a function of timing drift. Figure 4 shows SER as a function of $B_\tau T$ for a $n_R = 2$ QPSK system at $\bar{E}_s/N_0 = 12dB$ and $\bar{E}_s/N_0 = 16dB$. The

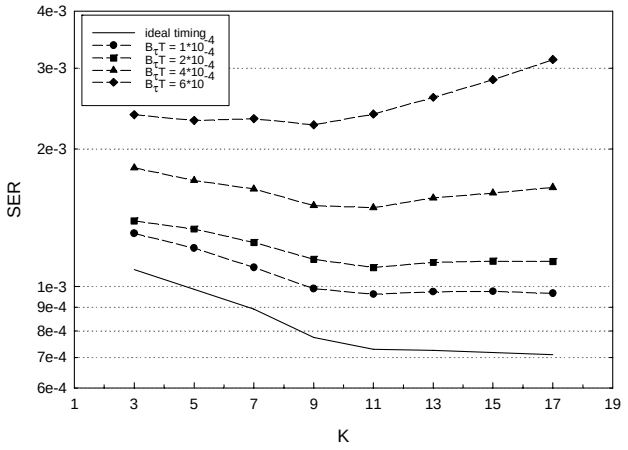

Fig. 3. SER vs number of interpolated pilots K (QPSK, $n_R = 2$, Wiener PSAM, $L_d = 8$, $\bar{E}_s/N_0 = 12dB$).

channel estimation was done via Wiener PSAM with $K = 9$ and pilot spacing of $L_f = 10$. Performance for a system with perfect channel knowledge is included for comparison, which correspond to a receiver with not decoding delay. In addition, in order to evaluate the effects of channel estimation errors separately from the effects of the delay, Figure 4 also shows results for ideal CSI where the timing information was delayed by the same amount as in the PSAM system.

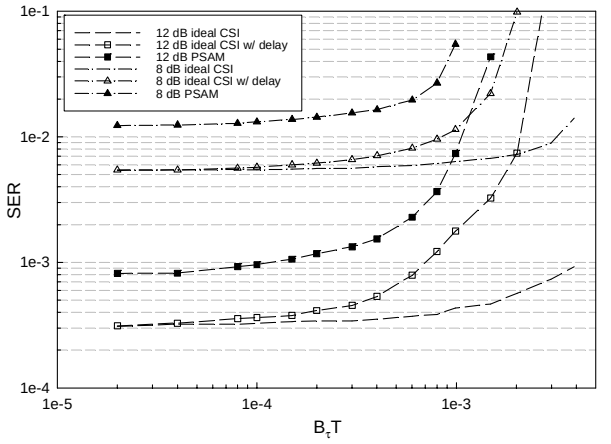

Fig. 4. SER vs $B_\tau T$ (QPSK, $n_R = 2$).

In the case of perfect channel knowledge and no delay, the system is able to track timing in excess of $B_\tau T = 2 \times 10^{-3}$. We see that this range decreases significantly with the introduction of the delay. The effect of channel estimation error results in further reduction in stable range. This effect is more pronounced for higher $\bar{E}_s/N_0$, and will manifest itself in an error floor in systems with faster timing drift.

We should point out that the tracking range can be increased by adjusting a number of system parameters. As shown by results of Section V-B, a lower K will improve the SER for faster timing drift. Also, for reasonably high SNR, the error threshold ϵ_{th} and the loop filter constant α can be decreased. This will result in a a more responsive timing loop, improving overall system performance.

VI. Conclusion

We have evaluated the performance of a robust timing error detector in tandem with PSAM-based channel estimation in frequency-flat Rayleigh fading MIMO system. The SER results show that the performance drop in comparison to ideal timing and channel knowledge case is mainly due to the channel estimation. The timing tracking produces no degradation in most of the SNR region for moderate values of timing bandwidth. We have demonstrated that the delay inherent to PSAM interpolation decreases the range of timing drift bandwidth successfully tracked by the receiver. An optimum value for the number of pilot interpolants was determined.

Acknowledgment

The authors would like to thank NSERC of Canada and the Bell Mobility / Samsung Grant on Smart Antennas at Queen's University for their support of this research.

References

[1] S.M.Alamouti. A simple transmit diversity technique for wireless communication. *IEEE J. Select. Areas Commun.*, 16(8):1451–1458, October 1998.

[2] V.Tarokh, N.Seshadri, and A.R.Calderbank. Space-time block coding for wireless communications: Performance criterion and code construction. *IEEE Trans Inf. Theory*, 44:744–765, March 1998.

[3] V.Tarokh, H.Jafarkhani, and A.R.Calderbank. Space-time block coding for wireless communications: Performance results. *IEEE J. Select. Areas Commun.*, 17:451–460, March 1999.

[4] S.Sampei and T.Sunaga. Rayleigh fading compensation method for 16QAM in digital land mobile radio channels. *Proceedings from 1989 IEEE Vehicular Technology Conference*, pages 640–646, May 1989.

[5] M.L.Moher and J.H.Lodge. TCMP - a modulation and coding strategy for Ricean fading channels. *IEEE Journal on Selected Areas in Communications*, 7(9):1347–1355, December 1989.

[6] J.K.Cavers. An analysis of pilot symbol assisted modulation for Rayleigh fading channels. *IEEE Transactions on Vehicular Technology*, 40(4):686–693, November 1991.

[7] N.Lo, D.D.Falconer, and A.U.H. Sheikh. Adaptive equalization adn diversity combining for mobile radio using interpolated channel estimates. *IEEE Transactions on Vehicular Technology*, 40:636–645, August 1991.

[8] X.Tang, M.Alouini, and A.J.Goldsmith. Effect of channel estimation error on M-QAM BER performance in Rayleigh fading. *IEEE Trans Commun.*, COMM-47:1856–1864, December 1999.

[9] A.F.Naguib, V.Tarokh, N.Seshadri, and R.Calderbank. A space-time coding modem for high-data-rate wireless communications. *IEEE J. Select. Areas Commun.*, 16(8):1459–1478, October 1998.

[10] Y.-C.Wu and S.C.Chan. On the symbol timing recovery in space-time coding systems. In *Proc. IEEE WCNC*, March 2003.

[11] Y.-C.Wu, S.C.Chan, and E.Serpedin. Symbol-timing synchronization in space-time coding systems using orthogonal training sequences. In *Proc. IEEE WCNC*, March 2004.

[12] P.A.Dmochowski and P.J.McLane. Robust timing epoch tracking for Alamouti space-time coding in flat Rayleigh fading MIMO channels. In *Proc. IEEE ICC*, May 2005.

[13] P.A.Dmochowski and P.J.McLane. On the properties of a robust timing error detector for Alamouti space-time coding in Rayleigh fading MIMO channels with randomly distributed timng drift. In *IEEE GLOBECOM 2005 (submitted)*.

[14] G.Ganesan and P.Stoica. Space-time block codes: A maximum SNR approach. *IEEE Trans Inf. Theory*, 47(4):1650–1656, May 2001.

[15] G.L.Stuber. *Principles of Mobile Communications*. Kluwer Academic Publishers, Boston, 2001.

[16] K.H.Mueller and M.Muller. Timing recovery in digital synchronous data receivers. *IEEE Trans Commun.*, COMM-24:516–531, May 1976.